Effect of Molybdenum Incorporation on the Structure and Magnetic Properties of Cobalt Ferrite

C. Orozco[1], A. Melendez[1,2], S. Manadhar[1], S. R. Singamaneni[3], Kongara M. Reddy[4], K. Gandha[5], I.C. Niebedim[5], and C. V. Ramana[1,2*]

[1]*Department of Mechanical Engineering, University of Texas at El Paso, El Paso, Texas 79968, USA*

[2]*Department of Metallurgical and Materials Engineering, University of Texas at El Paso, El Paso, Texas 79968, USA*

[3]*Department of Physics, University of Texas at El Paso, El Paso, Texas 79968, USA*

[4]*Department of Physics, Boise State University, Boise, Idaho 83725, USA*

[5]*Critical Materials Institute, Ames Laboratory, Ames, Iowa 50011, USA*

[*] Author to whom correspondence should be addressed; Email: rvchintalapalle@utep.edu; Tel: 1-915-747-8690; Fax: 1-915-747-5019

ABSTRACT

We report on the effect of molybdenum (Mo) incorporation on the crystal structure, surface morphology, Mo chemical valence state and magnetic properties of cobalt ferrite ($CoFe_2O_4$, referred to CFO). Molybdenum incorporated cobalt ferrite ($CoFe_{2-x}Mo_xO_4$, referred to CFMO) ceramics were prepared by the conventional solid-state reaction method by varying the Mo concentration in the range of x=0.0-0.3. X-ray diffraction studies indicate that the CFMO materials crystallize in inverse spinel cubic phase. Molybdenum incorporation induced lattice parameter increase from 8.322 to 8.343 Å coupled with a significant increase in density from 5.4 to 5.7 g/cm^3 was evident in structural analyses. Scanning electron microscopy imaging analysis indicate that the Mo incorporation induces agglomeration of particles leading to larger particle size with increasing x(Mo) values. Detailed X-ray photoelectron spectroscopic (XPS) analyses indicate the increasing Mo content with increasing x from 0.0 to 0.3. XPS confirms that the chemistry of Mo is complex in these CFMO compounds; Mo ions exist in the lower oxidation state (Mo^{+4}) for higher x while in a mixed chemical valence state (Mo^{+4}, Mo^{+5}, Mo^{+6}) for lower x values. From the temperature dependent magnetization, the samples show ferrimagnetic behavior including the pristine CFO. From the isothermal magnetization measurements, we find almost 2-fold decrease in coercive field (H_c) from 2143 Oe to 1145 Oe with the increase in Mo doping up to 30%. This doping dependent H_c is consistently observed at all the temperatures measured (4, 100, 200 and 300 K). Furthermore, the saturation magnetization estimated at 4 K and at 1.5 T (from M-H loops) goes through a peak at 92 emu/g (at 15% Mo doping) from 81 emu/g (pristine CFO), and starts decreasing to 79 emu/g (at 30% Mo doping). The results demonstrate that the crystal structure, microstructure, and magnetic properties can be tuned by controlling the Mo-content in the CFMO materials.

I. INTRODUCTION

Spinel ferrites, which contain iron oxide, are magnetic ceramics with a vast potential for numerous scientific and technological applications.[1-25] Spinel ferrite is chemically represented as $M^{2+}Fe_2^{3+}O_4$, where M and Fe are divalent and trivalent cations, respectively. The chemistry and physics of M and Fe cations dictate the electrical and magnetic properties of ferrites. Cobalt ferrite $CoFe_2O_4$ (CFO), one among these spinel ferrites, is the most useful hard ferrimagnetic material, which exhibits unique properties such as strong spin-orbit (L-S) coupling, high Curie temperature, high coercivity, high magneto-crystalline anisotropy, moderate saturation magnetization, large Kerr effect and Faraday rotation, good mechanical hardness and chemical stability.[1-7]

Cobalt ferrite based materials find attractive applications in microwave and spintronic devices, solar cells, magnetostrictive sensors, drug delivery, transducers, actuators, lithium batteries, super capacitors and memory devices for computers.[1-12] Currently, nanoparticles and nano-architectures of CFO-based materials are gaining tremendous interest in view of their ability to exhibit tunable electrical and magnetic properties, which could be exploited in numerous technological applications.[2,3,8,10] Furthermore, higher values of magnetostriction make CFO a potential candidate material for 'strain sensor and actuator' applications.[11] Cobalt ferrites can be combined with a piezoelectric/ferroelectric material resulting in the multiferroic/magnetoelectric hetero-structures for application in multifunctional and tunable magneto-electronic devices. However, the origin of a wide variety of properties of phenomena of CFO-based intrinsic, doped, or composite/hybrid materials is primarily associated with the structural arrangement and/or deliberate modification of the intrinsic structure by the dopant ions or materials at the interface.

Cobalt ferrite offers an excellent platform from solid state, crystallography and structural chemistry point of view. The cubic spinel structure in which the oxygen atoms are placed in a

cubic close-packed arrangement with the metal atoms residing at tetrahedral and octahedral sites, labeled as A and B sites, respectively, is the characteristic of CFO.[14] It is well known that altering the occupancies of the A and B sites can give rise to slight variations in the spinel structure, which can affect the corresponding nature and magnitude of super-exchange interactions namely, A−A, B−B, and A−B, of which the A−B interactions tend to be highly significant.[14] Furthermore, especially for magnetic and electrical properties tuning, a wide range of possibilities can arise by exhibiting reliable control over the distribution of Co^{2+} and Fe^{3+} cations among the A and B sites resulting in an intrinsically, electrically and magnetically tunable system. For instance, partial substitution of Fe^{3+} by rare earth (RE) ion, such as Er, Dy, La, Nd, Ho, leads to structural distortion in spinel structure which in turn induces strain and significantly modifies the electrical and dielectric properties.[2,6,9,12,16,17,19,26-28] In addition, it has been reported in the literature that inclusion of transition metal (TM) ion, such as Zn, Cu, Co and Cd, in ferrites increase the dielectric constant due to the formation of excess Fe^{2+} which eventually increase the hopping of electrons between Fe^{2+} and Fe^{3+}.[17,21,28]

Recently, substitution for Fe^{3+} in spinel ferrites has been gaining tremendous importance to design materials for utilization in high-density magnetic recording, enhanced memory storage, magnetic fluids, and catalyst applications.[2,6,9,12-19, 26-28] In general, the chemical and physical nature of the ion/dopant into CFO matrix allows tuning the final magnetic, dielectric and electrical characteristics.[13-25] Specifically, the degree of modification that can result in the properties and phenomena of CFO depends on the ionic radius, the electronic configuration of the substituting ion, its site preference (A versus B site), and the extent of distribution at the specific sites within the spinel structure.[15-17] The goal of the present work is to derive a comprehensive understanding of the molybdenum (Mo), which is a non-magnetic transition metal and with d^o electron

configuration, incorporation induced effects on the crystal structure, morphology, magnetic behavior, and dielectric and electrical transport properties of CFO.

The impetus for the present work is twofold. Understanding the fundamental aspects of non-magnetic Mo incorporation on the structure and properties of CFO is the first. It has been already recognized that, among many possible ways of engineering the advanced functional materials based on ferrites, doping with different RE/TM-ions is a well-adopted, straightforward and versatile way to tune the structure and properties.[2,5,6,9,12,16-20] Depending on the ionic size and concentration, incorporation of RE/TM-ions in spinel ferrite results in an improved dielectric constant, increase in resistivity and a decrease in dielectric and magnetic losses. [2,5,16-20] However, understanding the effect of a refractory metal, such as Mo in this case, incorporation on the structure and the extent to which the electrical, magnetic and dielectric properties of CFO can be tuned is of primary interest in this work. Such a detailed understanding of Mo incorporation might allow further opportunities to tailor the CFO-based materials' behavior for selective applications where the thermal and chemical stability becomes important. Refractory metals are usually known for high temperature tolerance and mechanical stability[29-31]; thus, their incorporation might enhance the overall temperature stability of the CFO and could be more attractive for future applications, such as advanced sensors and photo-catalysis. Especially, Mo is known for its mechanical, protective, high-temperature stability and heat-resistance capabilities[30,31]; therefore, Mo-incorporation into CFO is ideal for designing materials for memory devices, sensors and actuators operating at elevated temperatures. The second driving factor for this work, as well as primary objective, is to derive a fundamental understanding of the ability of Mo-incorporation on the tunability of the CFO properties. First of all, it should be noted that the overall attention paid towards Mo incorporation into CFO is meager. There has been only a very little work reported in

the literature on the properties of non-magnetic Mo incorporated CFO.[32-34] Furthermore, while there exists very few efforts, fundamental understanding of the structure-composition-property relation in Mo-incorporated CFO is missing at this time. Additionally, although still some unanswered, fundamental scientific questions exists, recently observed and/or predicted ferroelectric/multiferroic character of Mo incorporated CFO is promising for future applications in magneto-electronics.[32,34] Thus, a better understanding of the combined structural, magnetic, dielectric and transport properties of CFMO is highly beneficial to tune the properties for desired electronic and electromagnetic applications. In this context, efforts in this work were directed to synthesize Mo incorporated CFO with the chemical formula $CoFe_{2-x}Mo_xO_4$ (x=0.0-0.3) by solid state reaction and to study their structure, chemistry, surface morphology and magnetic properties. Interestingly, as presented and discussed in this paper, the results demonstrate a significant and remarkable effect of Mo incorporation on the structure and magnetic properties of CFO. Based on the results, a chemistry(Mo)-structure(CFO)-magnetic property correlation in CFMO compounds is established.

II. EXPERIMENTAL DETAILS

The $CoFe_{2-x}Mo_xO_4$ (x=0.0-0.3) ceramics were prepared by the conventional solid-state reaction method. Cobalt oxide (CoO, 99.5%; NOAH Tech., USA) Iron Oxide (Fe_2O_3, 99.95%; NOAH Tech., USA) and molybdenum oxide (MoO_3, 99.5%; Alfa Aesar, USA) powders were used. The powders were mixed by agate mortar and pestle in ethanol for 2 h. After drying, the mixtures were calcined at 1200 °C for 12 h. Then the powder was mixed with 5 wt% polyvinyl alcohol (PVA) solution and then pressed into pellets in a Carver press into disk specimens with a diameter of ~7.8 mm and a thickness of ~1.5 mm under 5-ton pressure. The disks were sintered at 1300 °C

for 6 h in air in a box furnace with heating and cooling rates of 10 ˚C/min. Phase identification and crystal structure of the materials synthesized were investigated using X-ray diffraction (XRD) measurements employing a Bruker D8 Discover X-ray diffractometer. Measurements were made at room temperature using Cu Kα radiation (λ=1.5406 Å). Surface morphology of CFMO compounds was examined by scanning electron microscopy (SEM). The microstructures were observed with the scanning electron microscope (SEM; Hitachi TM1000). The chemical analysis of CFMO samples, specifically the chemical state of Mo has been determined using a Physical Electronics Versaprobe X-ray photoelectron spectroscopy (XPS) system. The system utilizes a Mg *Kα* radiation (1253.6 eV) source. The binding energy was calibrated with reference to the C 1*s* level of carbon (285 eV). Survey scans as well as high energy resolution scans were obtained for a detailed chemical analysis of the samples. CasaXPS software was used for atomic composition and peak fitting analysis. To fit the high energy resolution spectra, Gaussian-Lorentzian line shapes were used along with Shirley background subtraction for accurate peak area determination. The superconducting quantum interference device (SQUID) and versalab VSM were employed to perform magnetization measurements with a sensitivity of 10^{-7} emu.

III. RESULTS AND DISCUSSION

A. Crystal Structure and Chemical State – XRD and XPS

XRD patterns of pure CFMO (*x*=0.0-0.3) are shown in Fig. 1. XRD data indicate that the CFMO crystallizes in the inverse spinel phase without any impurity phase. The peaks observed and their assignment are as indexed in Fig. 1. The lattice constant determined from XRD for pure CFO is 8.322 Å, which agrees with that of pure $CoFe_2O_4$ reported in the literature.[3,4] The remarkable effect of Mo incorporation is reflected in two important observations in XRD analyses.

An increase in the lattice constant is the first and an increase in the average crystallite size is the later. Lattice constant increases from 8.322 Å (*x=0.0*) to 8.343 Å (*x=0.3*) with increasing Mo-content. The corresponding crystallite size increases from ~50 nm (*x*=0.0) to 85 nm (*x*=0.3). Differences in the ionic radii of Co, Fe, Mo ions can result in lattice strain which account for the lattice parameter and, hence, unit cell expansion. Such effect is mainly due to the larger Mo ion substitution for Fe^{3+} in CFO. The lattice parameter, density and average size values determined from XRD are listed in Table I.

The variation of lattice parameter (*a*) with Mo content is shown in Fig. 2. It can be noted that plot exhibits *x-a* linear relationship, although almost appears to be saturated for $x \geq 0.2$. The observed *x-a* trend in CFMO indicates the continuous increase in lattice parameter with Mo content. It is obvious that when some of Fe^{3+} ions are substituted by Mo^{y+} ions (*y*=3,4, 5 and 6), the lattice is subjected to distortion resulting in an increase or decrease in the lattice parameter. Note that the chemistry i.e., the chemical state of Mo, is always complex due to the possibility of Mo ions exist in variable chemical valence states, namely Mo^{3+}, Mo^{4+}, Mo^{5+}, Mo^{6+}.[35-39] Therefore, the lattice parameter increase or decrease or a reasonable compromise is due to the net result of two effects. Having large ionic radius than Fe^{3+} (0.645 Å), lower valence states of Mo^{y+} (*y*=3,4,5) incorporation into the structure induces distortion leading to the increased lattice parameter. On other hand, if some of the Mo ions did not substitute for Fe in the cubic structure but formed another distorted or secondary phase, then the lattice parameter might decrease. The major effect of Mo-substitution in CFO is, thus, lattice expansion due to the larger ionic radius of Mo ions. However, note that there are differences in the ionic radius when that of Fe^{3+} is compared with either Mo^{3+} or Mo^{6+}. The ionic radius of Fe^{3+}(0.64 Å) is smaller than that of Mo^{3+} (0.69 Å) and larger than that of Mo^{6+}(0.59 Å). Therefore, the lattice parameter increase with increasing Mo

content indicates the characteristic of Mo ions entering into CFO must be in their lower valence state than Mo^{6+} state because that is the only way that lattice expansion can occur. Thus, the present data clearly indicate that the Mo exists in lower chemical state(s) while replacing/substituting for Fe^{3+} in the CFO lattice. The trend of lattice expansion or contraction with progressive Mo content is, however, not very clear in the literature. For instance, Mohamed et al. reported lattice constant increase from 8.3813 Å to 8.3991 Å in Mo substituted CFO, where Mo content was varied from 0 to 30% (x=0.00-0.30).[33] On the other hand, Heiba et al. reported a lattice parameter contraction from 8.360 Å to 8.323 Å for Mo incorporated CFO ($CoFe_{2-x}Mo_xO_4$) for a similar range of composition (x=0.00-0.30).[34] However, the effect of Mo incorporation is evident from XRD analyses of CFMO materials in this work; CFMO exhibit lattice parameter enhancement from 8.322 Å (x=0.0) to 8.343 Å (x=0.3) due to the larger ionic radius of lower valence state Mo ions compared to Fe^{3+}. In order to further validate this hypothesis and also to confirm the chemical state of Mo ion in these CFMO compounds, chemical analysis has been made by the Mo core-level XPS data. The detailed XPS spectra of Mo 3*d* region of the CFMO samples are shown in Fig. 3. While the peak intensity is not appreciable for samples with low Mo content (x) and also due scattering losses due to powdered sample nature, the intensity Mo 3*d* peak increases with increasing x. It is evident that, for highest Mo concentration i.e., CFMO (x=0.30), the Mo 3*d* doublet (due to spin-orbit splitting; j=5/2 and j=3/2) are clearly resolved with a spin-orbit splitting energy separation, ΔE(Mo 3*d*), of 3.2 eV. Both the Mo $3d_{5/2}$ and Mo $3d_{3/2}$ peaks show a weak but pronounced shoulder contribution from the lower binding energy (BE) side. Therefore, the component analysis was performed by considering the peak as superposition of two doublets shifted in energy but with the same intensity ratio of the components and spin-orbit splitting. Most notable feature is the fact that the evolved Mo 3*d* scan is rather broad in nature, which is due to Mo ions existing in multiple

valence states.[39] Note that the Mo chemistry is complex due its ability to take chemical valence states ranging from 2+ to 6+.[35-39] The peak fitting procedure confirms that the Mo ions indeed exists in Mo^{6+}, Mo^{5+} and Mo^{4+} states. The Mo $3d_{5/2}$ component located at a BE of 232.51 eV corresponds to Mo^{+6} while the Mo$3d_{5/2}$ component located at 231.17 eV is assigned to Mo^{+5}. The Mo 3*d* doublet components (Mo $3d_{5/2}$ and Mo $3d_{3/2}$) resolved and their respective peak positions can be assigned to Mo^{+6} and Mo^{+5} without any ambiguity. However, the other doublet component, which evolves only for samples with higher Mo content is the Mo peak at a much lower BE which is due to the presence of Mo in lower oxidation state (Mo^{+4}) at the expense of Mo^{+6}. In all the CFMO samples, presence of Mo^{+4} evolves at higher Mo concentration or as Mo concentration increases steadily to higher values (>0.2). According to literature, the component peaks at 230.1 eV and 233.1 eV, respectively, are assigned to Mo $3d_{5/2}$ and Mo$3d_{3/2}$, respectively, characterizing the chemical state of Mo^{+4}.[35,39] Thus, the XPS analyses confirm the presence of Mo in lower valence states, namely Mo^{+4} and Mo^{+5}, which we believe are primarily responsible for the observed lattice expansion in XRD studies of CFMO compounds.

The density of the samples was also calculated from XRD data. The following equations were employed:

$$a = [d^2(h^2 + k^2 + l^2)]^{1/2} \quad (1)$$

$$V = a^3 \quad (2)$$

$$\rho_{eff} = \frac{nM}{Na^3} \quad (3)$$

where M is the molecular weight, N is the Avogadro number, n is the number of formula units per unit cell, m is the mass, r is the radius and h is the thickness of the pellet. The density variation of CFMO compounds with Mo context (*x*) is shown in Fig. 4. It is evident that ρ_{xrd} increases with increasing Mo content (*x*). The two important general remarks that can be derived from density

variation of CFMO compounds are as follows. Effective incorporation of Mo into CFO and completeness of the sintering process to the best possible extent is the first. Later is the density increase with Mo concentration. The density and atomic weight of Mo^{3+} are 10.28 g/cm^3 and 95.94, which are greater than those of Fe^{3+} 7.874 g/cm^3 and 55.845. Thus, the overall density increase of CFMO compounds can attributed to the fact that the density and atomic weight of Mo are higher than those of Fe for which the Mo ions are substituting/replacing in CFO. Rahman et. al. reported similar behavior with the incorporation of Gd into CFO and interpreted such density increase are due to density and atomic weight of Gd is larger than that of Fe.[12] However, on the other hand, it can be noted that there is a difference in theoretical density and effective density (Table I) of the CFMO compounds which might be due to the small percentage of pores and/or atomic scale defects, which cannot be avoided in ceramics fabricated by high temperature solid state ceramic processes. Finally, to understand the effect of Mo on the crystal growth and kinetics, the variation in average crystallite size of the CFMO samples was considered. The crystallite size (*d*) was calculated from the integral width of the diffraction lines using the Scherrer's equation after background subtraction and correction for instrumental broadening.[40] The Scherrer equation[40] is:

$$d = 0.9\lambda/\beta\cos\theta \qquad (4)$$

where *d* is the grain size, λ is the wavelength of X-rays, β is the width of a peak at half of its intensity, and θ is the angle of the peak. The variation of crystallite size with *x*(Mo) is presented in Fig. 5. It can be noted that the crystallite size is in the range of 40-54 nm for CFMO materials. It is important to recognize that the Mo incorporation induces the crystallite size increase, which can be due to difference in the ionic radius of Mo compared to Fe in CFMO. Since the difference in ionic radius Mo replacing or substituting for Fe in CFO is relatively large, higher content (*x*) of Mo doping results in mobility differences, which results in the average size increases as well as

agglomeration of smaller crystallites to contribute to the grain growth as noted in SEM analyses as presented below.

B. Morphology – SEM

The SEM data of CFMO ceramics are shown in Fig. 6 as a function of Mo content. It is evident from these images that grain size increases with increasing Mo content. Perhaps, Mo incorporation facilitating the more number of particles joining together leading to the formation of larger size particles. The particle size was estimated by the linear intercept method (ASTM method), which showed that increasing Mo content increases the size from ~4 to 11 μm. We speculate that the chemistry behind the observed increase in grain size with Mo incorporation may be due to the difference in ionic radii of Mo and Fe ions. In addition, Mo existing in variable chemical valence states may also contribute such enhancement in particle size. Since the difference in ionic radius Mo replacing or substituting for Fe in CFO is relatively large, higher content (x) of Mo doping results in mobility differences, which results in the observed growth. Perhaps, digestion of Mo ions into CFO in place of Fe atoms causes the distortion within the grain as well as at grain boundaries for higher doping concentration causes the lattice expansion and grain growth. Such differences in morphology evolution were also noted in Hf-Zr mixed oxides, where the distortion due to Zr^{4+} ions replacing the Hf^{4+} ions was noted.[41] In addition, Venkata Ramana et al. have recently reported the effect of Fe-doping on the grain growth behavior of of $(Ba_{0.85}Ca_{0.15})(Ti_{0.9}Zr_{0.1})O_3$ synthesized by a chemical route.[42] The difference in the ionic radii of Ti^{4+} and Fe^{3+} ions was accounted for the differences in grain growth behavior upon Fe doping.[42]

C. Magnetism – SQUID and VSM

The magnetization measurements were performed using a SQUID magnetometer on a small speck (of known weight) of a pellet made from the polycrystalline samples of CFO, in which, the Mo is doped up to 30% on Fe site. Figure 7 plots the temperature dependent zero-field cooled spontaneous magnetization data measured (at 200 Oe) from 0, 10, 15, 20 and 30 % Mo doped CFO samples. These measurements were made during the heating cycle after the samples were cooled down to 4K. For all the samples, we noticed that the magnetic moment decreases while samples are being cooled. The data infer that these samples show ferrimagnetic behavior, consistent with the previous published work.[32]

Figure 8 (a-f) presents the isothermal magnetic behavior (M-H) collected at 4,100,200 and 300K of all the samples (0, 5, 10, 15, 20, 30% Mo doped CFO) studied in this work, as a function of Mo doping, ranging from 0-30%, respectively. Three salient features can be noted: (a) the hysteresis loops are in agreement with the ferrimagnetic behavior, i.e.) the magnetization increases linearly at high field, (b) the M-H loop starts decreasing as the temperature increased (4-300 K) for all the samples, (c) the coercive field starts decreasing monotonically as a function of increasing temperature and Mo doping, (d) the saturation magnetization shows non-monotonic behavior peaking at 15% Mo doping. It can be readily noted that the ferrimagnetic nature retains up to room temperature in all the samples, though the magnetic hysteresis decreased as the samples warmed up. In addition, it is observed that the saturation magnetization (M_s) is almost independent of temperature, unlike the coercive field (H_C), which is strongly temperature-dependent. This is consistently noted in all the samples studied here. These are the hallmark signatures of ferrimagnetic materials[32].

In Fig. 9, we show the variation of coercive field H_c (left Y-axis) and saturation magnetization M_s (right Y-axis) collected from M-H data at 4K as a function of Mo doping (0-

30%) in CFO. As stated before, the H_c is found to decrease with the increase in Mo doping. This is expected for any ferrimagnetic material due to the dilution of magnetic lattice as a function of doping with non-magnetic element such as Mo. Also, most likely, the decrease in coercivity is associated with the reduction in anisotropy with the increase in Mo doping in CFO. Interestingly, on the other hand, M_s shows a non-monotonic behavior as a function of Mo doping. First, M_s decreases marginally from 83 to 82 emu/g (upon 5% Mo doping) and then increases strongly showing a peak (at 91 emu/g) at around 15% of Mo doping before it decreases again as the doping increases further. The same trend in H_c and M_s has been observed at all the temperatures measured. The observed H_c in our sample is consistent with previous observations reported (~ 2000 -2500 Oe) on CFO powders and thin films.[43] In the case of RE element (Er, Nd) doped CFO, H_c increased sharply at the low doping and stayed constant at further higher doping level (0-4%), and argued to be due to strong spin-orbit coupling of rare-earth elements.[8,44-46] Similar to the present work, the Zn doped CFO shows decrease in coercivity (525-165 Oe) as a function of doping (0-10%).[47] While we do not have a definite experimental evidence to show whether Mo enters into tetrahedral or octahedral site in CFO lattice, this issue is still under discussion in the literature[32,48]. In their previous work, the authors in ref [32] reported that Mo occupies tetrahedral position in CFO lattice. After about 5 years later, in contradiction, the same group reported[48] that it goes into octahedral site using neutron diffraction study. This is partly due to the complex substitutional nature of Mo cations. While it is hard to pinpoint the exact mechanism(s) for the doping dependent magnetic behavior, our combined experimental findings led us to believe that the complex magnetic exchange interactions between the guest (Mo^{+4}, Mo^{+5}, Mo^{+6}) and the host (Fe^{3+}, $Co^{2+)}$ transition metal ions could be at play. In addition, one has to consider their strong spin-orbit coupling, and corresponding magneto crystalline anisotropy to account for doping dependent magnetic behavior.

To get additional insights, neutron diffraction measurements are being planned. The present study coupled with literature works shows that CFO exhibits distinct magnetic properties when CFO is doped with transition metal elements such as Mo, Zn and rare-earth elements such as Er, Nd and Dy.

IV. SUMMARY AND CONCLUSIONS

The effect of molybdenum (Mo) incorporation on the crystal structure, surface morphology, and magnetic properties of cobalt ferrite has been investigated in detail. The intrinsic and Mo-incorporated CFO crystallizes in inverse spinel cubic phase. Significant increase in density from 5.4 to 5.7 g/cm^3 with Mo-incorporation is attributed to the higher atomic mass of Mo. The chemistry of Mo is complex. The Mo ions exist in the lower oxidation state (Mo^{+4}) for higher *x* while it exists in mixed chemical valence state (Mo^{+4}, Mo^{+5}, Mo^{+6}) for lower *x* values. The difference in ionic radius between Mo, especially those in lower valence states, and Fe ions in the host CFO lattice causes the lattice parameter increase from 8.322 to 8.343 Å. The ionic and atomic mass difference also induces the agglomeration of particles leading to larger grain size with increasing *x*(Mo) in CFMO. The temperature dependent magnetization data indicates that the studied samples show ferrimagnetic nature. The isothermal magnetization measurements indicate almost a 2-fold decrease in coercive field (H_c) from 2143 Oe to 1145 Oe with the increase in Mo-content. The Mo-induced effect on H_c of CFMO samples is also evident and consistent in the temperature (4-300 K) dependent measurements. The saturation magnetization exhibits a peak value of 92 emu/g at x(Mo)=0.15 and finally decreases to 79 emu/g at x(Mo)=0.30. The results demonstrate that the crystal structure, morphology, and magnetic properties can be tuned by controlling the Mo-content in the CFMO ceramics.

Acknowledgements

The authors acknowledge with pleasure the support from the National Science Foundation (NSF), USA, with NSF-PREM grant #DMR-1205302. One of us, SRS, acknowledges support from UTEP-start up grant. The work at Ames Laboratory was supported by the Critical Materials Institute, an Energy Innovation Hub funded by the U.S. Department of Energy, Office of Energy Efficiency and Renewable Energy, Advanced Manufacturing Office.

References

(1) Spaldin, N. A.; Fiebig, M. The renaissance of magnetoelectric multiferroics. *Science* **2005**, *309*, 391–392.

(2) Kakade, S.G.; Kambale, R.C.; Kolekar, K.; Ramana, C.V. Dielectric, complex impedance, and electrical transport properties of erbium (Er^{3+}) ion-substituted nanocrystalline, cobalt-rich ferrite ($Co_{1.1}Fe_{1.9-x}Er_xO_4$). *J. Phys. Chem. C* **2016**, *113*, 9070-9076.

(3) Mazario, E.; Menéndez, N.; Herrasti, P.; Cañete, M.; Connord, V.; Carrey, J. Magnetic hyperthermia properties of electrosynthesized cobalt ferrite nanoparticles. *J. Phys. Chem. C* **2013**, *117*, 11405-11411.

(4) Ramana, C. V.; Kolekar, Y. D.; Bharathi, K. K. ; Sinha, B.; Ghosh, K. Correlation between structural, magnetic, and dielectric properties of manganese substituted cobalt ferrite. *J. Appl. Phys.* **2013**, *114*, 183907.

(5) Kambale, R. C.; Song, K. M.; Koo, Y. S.; Hur, N. Low temperature synthesis of nanocrystalline Dy doped cobalt ferrite: Structural and magnetic properties. *J. Appl. Phys.* **2011***, 110,* 053910.

(6) Prathapani, S.; Monaji, V. R.; Jayaraman, T. V.; Das D. Structural and ambient/sub-ambient temperature magnetic properties of Er-substituted cobalt-ferrites synthesized by sol-gel assisted auto-combustion method. *J. Appl. Phys.* **2014***, 116*, 023908(1-9)

(7) Valenzuel, R. Novel application of soft ferrites. *Phys. Res. Inter.* **2012***, 591839***,** 1-9.

(8) Mukherjee, D.; Hordagoda, M.; Hyde, R.; Bingham, N.; S.; Hariharan, Witanachchi, S.; Mukherjee, P. Nanocolumnar interfaces and enhanced magnetic coercivity in preferentially oriented cobalt ferrite thin films grown using oblique-angle pulsed laser deposition. *ACS Appl. Mater. Interfaces* **2013**, 5, 7450-7457.

(9) Kamala Bharathi, K.; Markandeyulu, G.; Ramana, C. V. Structural, magnetic, electrical, and magnetoelectric properties of Sm- and Ho-substituted nickel ferrites. *J. Phys. Chem. C* **2011**, *115*, 554-560.

(10) Agnė Mikalauskaitė, Rokas Kondrotas, Gediminas Niaura, Arūnas Jagminas. Gold-coated cobalt ferrite nanoparticles via methionine-induced reduction. *J Phys. Chem. C* **2015**, *119,* 17398-17407.

(11) Monaji, V. R.; Das, D. Influence of Zr doping on the structural, magnetic and magnetoelastic properties of cobalt- ferrites. *J. Alloys Compd.* **2015***, 634,* 99–103.

(12) Rahman, Md. T.; Vargas, M.; Ramana, C.V. Structural characteristics, electrical conduction and dielectric properties of gadolinium substituted cobalt ferrite, *J. Alloys Compd.* **2014,** *617,* 547–562.

(13) Kahn, M. L.; Zhang, Z. J. Synthesis and magnetic properties of $CoFe_2O_4$ spinel ferrite nanoparticles doped with lanthanide ions. *Appl. Phys. Lett.* **2001***, 78*, 3651-3653.

(14) Pandit, R.; Sharma, K. K.; Kaur, P.; Kumar, R. Cation distribution controlled dielectric, electrical and magnetic behavior of Ln^{3+} substituted cobalt ferrites synthesized via solid-state reaction technique. *Mater. Chem. Phys.* **2014***, 148,* 988-999.

(15) Mahalakshimi, S.; Srinivasa M. K.; Nithiyanantham, S. Electrical properties of nanophase ferrites doped with rare earth ions. *J. Supercond. Nov. Magn.* **2014**, *27,* 2083-2088.

(16) Dascalu, G.; Popescu, T.; Feder M.; Caltun, O. F. Structural, electric and magnetic properties of $CoFe_{1.8}RE_{0.2}O_4$ (RE=Dy,Gd,La) bulk materials. *J. Magn. Magn. Mater*. **2013**, *333*, 69-74.

(17) Bharathi, K. K.; Ramanaa, C. V. Improved electrical and dielectric properties of La-doped Co ferrite. *J. Mater. Res.* **2011***, 26*, 584-591.

(18) Alcantara, G. B.; Paterno, L. G.; Fonseca, F. J.; Pereira-da-Silva, M. A. ; Morais, P. C.; Solera, M. A. G. Dielectric properties of cobalt ferrite nanoparticles in ultrathin nanocomposite films. *Phys. Chem. Chem. Phys.* **2013***, 15,* 19853-19861.

(19) Pervaiz, E.; Gul I. H. Structural, electrical and magnetic studies of Gd^{3+} doped cobalt ferrite nanoparticles. *Int. J. Curr. Eng. Technol.* **2012***, 2*, 377-387.

(20) Kadam, A. A.; Shinde, S. S.; Yadav, S. P.; Patil, P. S.; Rajpure, K. Y. Structural, morphological, electrical and magnetic properties of Dy doped Ni–Co substitutional spinel ferrite. *J. Magn. Magn. Mater*. **2013**, *329,* 59–64.

(21) Kolekar, Y. D.; Sanchez, L.; Rubio, E. J.; Ramanan, C. V. Grain and grain boundary effects on the frequency and temperature dependent dielectric properties of cobalt ferrite–hafnium composites. *Solid State Comm.* **2014**, *184***,** 34–39.

(22) Naik, S. R.; Salker, A. V. Change in the magneto structural properties of rare earth doped cobalt ferrites relative to the magnetic anisotropy. *J. Mater. Chem.* **2012***, 22,* 2740-2750.

(23) Prathapani, S.; Monaji, V. R.; Jayaraman, T. V. ; Das, D. Structural and ambient/sub-ambient temperature magnetic properties of Er-substituted cobalt-ferrites synthesized by sol-gel assisted auto-combustion method. *J. Appl. Phys.* **2014***, 116,* 023908(1-9).

(24) Murugesan, C.; Chandrasekaran, G. Dielectric relaxations and alternating current conductivity in manganese substituted cobalt ferrite. *RSC Adv.* **2015,** *5*, 73714-73725.

(25) Shobana, M.K.; Nam, W.; Choe, H. Yttrium doped cobalt nanoferrites prepared by sol-gel combustion and their characterization. *J. Nanosci. Nanotechnol.* **2013,** *13*, 3535-3538.

(26) Gu, Z.; Xiang, X.; Fan, G.; Li, F. *J. Phys. Chem. C* **2008**, *112*, 18459-18466.

(27) Cheng, F.; Liao, C.; Kuang, J.; Xu, Z.; Yan, C.; Chen, L.; Zhao, H.; Liu, Z. *J. Appl. Phys.* **1999**, 85, 2782-2786.

(28) Lee, S. J.; Lo, C. C. H.; Matlage, P. N.; Song, S. H.; Melikhov, Y.; Snyder J. E.; Jiles, J. C. *J. Appl. Phys.* **2007**, *102*, 073910.

(29) Bauccio, M. *Refractory Metals*. 1993, *ASM Metals Reference Book*, ASM International, pp. 120–122.

(30) Habashi, F. Historical introduction to refractory metals. *Miner. Process. Ext. Metall. Rev.* **2008**, *22*, 25-53.

(31) Davis, J. R. *Heat-Resistant Materials.* **1997**, ASM International.

(32) Dwivedi, G. D.; Tseng, K. F.; Chan, C. L.; Shahi, P.; Lourembam, J.; Chatterjee, B.; Ghosh, A. K.; Yang, H. D.; Sandip Chatterjee. Signature of ferroelectricity in magnetically ordered Mo-doped $CoFe_2O_4$. *Phys. Rev. B* **2010**, *82*, 134482.

(33) Mohamed, M.B.; Wahba, A.M.; Yehia, M. Structural and magnetic properties of $CoFe_{2-x}Mo_xO4$ nanocrystalline ferrites, Mater. Sci. Eng. B **2014**, *190*, 52-58.

(34) Heiba, Z.K.; Mostafa, N.Y.; Abd-Elkader, Omar. H. Structural and magnetic properties correlated with cation distribution of Mo-substituted cobalt ferrite nanoparticles. *J. Magn. Magn. Mater.* **2014**, *368*, 246-251.

(35) Choi, J. G.; Thompson, L. T. XPS Study of as-Prepared and Reduced Molybdenum Oxides. *Appl. Surf. Sci.* **1996**, *93* (2), 143–149.

(36) Ramana, C. V.; Atuchin, V. V.; Pokrovsky, L. D.; Becker, U.; Julien, C. M. Structure and Chemical Properties of Molybdenum Oxide Thin Films. *J. Vac. Sci. Technol. A* **2007**, *25* (4), 1166–1171.

(37) Ramana, C. V.; Atuchin, V. V.; Kesler, V. G.; Kochubey, V. a.; Pokrovsky, L. D.; Shutthanandan, V.; Becker, U.; Ewing, R. C. Growth and Surface Characterization of Sputter-Deposited Molybdenum Oxide Thin Films. *Appl. Surf. Sci.* **2007**, *253*, 5368–5374.

(38) Bhachu, D. S.; Scanlon, D. O.; Sankar, G.; Veal, T. D.; Egdell, R.G.; Cibin, G.; Dent, A.J.; Knapp, C. E.; Carmalt, C. J.; Parkin, I.P. Origin of high mobility in molybdenum-doped indium oxide, *Chem. Mater.* **2015**, *27*, 2788-2796.

(39) Silipingi, L.; Barreca, F.; Fazio, E.; Neri, F.; Spano, T.; Piazza, S.; Sunseri, C.; Inquanta, R., Template electrochemical growth and properties of Mo oxide nanostructures, *J. Phys. Chem. C* **2014**, *118*, 22299−22308.

(40) Cullity, B.D.; Stock, S.R. *Elements of X-ray Diffraction*, **2001**, Prentice Hall.

(41) Noor-A-Alam, M.; Choudhuri, A.R.; Ramana, C.V. Effect of composition on the growth and microstructure of hafnia–zirconia based coatings, *Surf. Coat. Technol.* **2011**, *206*, 1628-1633.

(42) Venkata Ramana, E.; F. Figueiras, F.; Mahajan, A.; David Maria Tobaldi; Costa, B.F.O.; Graça, M. P. F.; Valente, M. A. Effect of Fe-doping on the structure and magnetoelectric properties of $(Ba_{0.85}Ca_{0.15})(Ti_{0.9}Zr_{0.1})O_3$ synthesized by a chemical route. *J. Mater. Chem. C* **2016**, *4*, 1066-1079.

(43) Lee J G; Lee H M; Kim C S; Oh Y J; Magnetic properties of $CoFe_2O_4$ powders and thin films grown by a sol-gel method, *J. Mag. Mag. Mat.*, **1998**, *177*, 900-902.

(44) Yadav R. S.; Havlica J, Masilko J; Kalina L; Wasserbauer J; Hajdúchová M; Enev V; Kuřitka I; Kožáková Z; Impact of Nd3þ in $CoFe_2O_4$ spinel ferrite nanoparticles on cation distribution, structural and magnetic properties, *J. Mag. Mag. Mat.* **2016,** *399*,109–117.

(45) Burianova S; Vejpravova J P, Holec P; Plocek J; and Niznansky D, Surface spin effects in La-doped $CoFe_2O_4$ nanoparticles prepared by microemulsion route, *J. Appl. Phys.* **2011,***110*, 073902.

(46) Zhao L; Yang H; Zhao X; Yu L; Cui Y; Feng S; Magnetic properties of $CoFe_2O_4$ ferrite doped with rare earth ion, *Mater. Lett.* **2006,** *60*, 1 – 6.

(47) Somaiah N, Jayaraman T V; Joy P.A; and Das D, Magnetic and magnetoelastic properties of Zn-doped cobalt-ferrites-$CoFe_{2-x}Zn_xO_4$ (x = 0, 0.1, 0.2, and 0.3), *J. Mag. Mag. Mat.* **2012**, *324*, 2286–2291.

(48) A. Das, G.D.Dwivedi, Poonam Kumari, P. Shahi, H. D. Yang, A. K. Ghosh, Sandip Chatterjee Neutron diffraction study of multiferroic Mo-doped $CoFe_2O_4$; Journal of Magnetism and Magnetic Materials 379 (**2015**) 6–8

Figure Captions

Figure 1 XRD patterns of the $CoFe_{2-x}Mo_xO_4$ (CFMO) ferrites as a function of *x*. The peaks identified and their assignment are as indicated. The data indicate that the CFOM crystallize in inverse spinel structure.

Figure 2 Variation of lattice parameter with Mo concentration (*x*). Molybdenum incorporation induced lattice expansion compared to that of pure CFO (*x*=0) is evident.

Figure 3 XPS core-level scans of Mo 3*d* in CFMO samples. The Mo peak is absent in CFO(x=0). The peak intensity is not appreciable at the beginning of Mo incorporation but evolves into broader peak with increasing Mo content. The broader peak can be resolved into components, which can be assigned to Mo in 4+, 5+ and 6+ valence states.

Figure 4 Density variation of CFMO ceramics with Mo content. The linear increase in density is due to the incorporation of heavier Mo substituting for Fe in the CFO.

Figure 5 The variation of average crystallite size in CFMO. The crystallite size increase with increasing Mo content in CFMO is evident.

Figure 6 Surface morphology of CFMO samples. Molybdenum incorporation induced agglomeration to increase grain size with *x* is evident in these micrographs.

Figure 7 The temperature dependence of spontaneous magnetization (M-T curve, 4-350 K) collected from CFMO, with Mo percentage of 0, 10, 15, 20, and 30 %. The measurements were made during the heating cycle after the samples were cooled down to 4K under zero magnetic field, measured at 200 Oe. The data infer the ferrimagnetic nature of the samples.

Figure 8 The isothermal magnetization response measured at 4, 100, 200, and 300K from CFMO polycrystalline samples prepared with Mo = 0% (a), Mo = 5% (b), Mo = 10% (c), 15% (d), 20% (e), and 30% (f). It can be readily noted that the ferrimagnetism is retained in all the samples as it is reflected from the high magnetic field liner slope.

Figure 9 The variation of coercive field H_c (left Y-axis) and saturation magnetization M_s (right Y-axis, measured from M-H curves) at 4K as a function of Mo doping (0-30%) in CFO. The H_c is found to decrease with the increase in Mo doping. Interestingly, M_s shows a peak at around 15% of Mo doping.

Figure 1

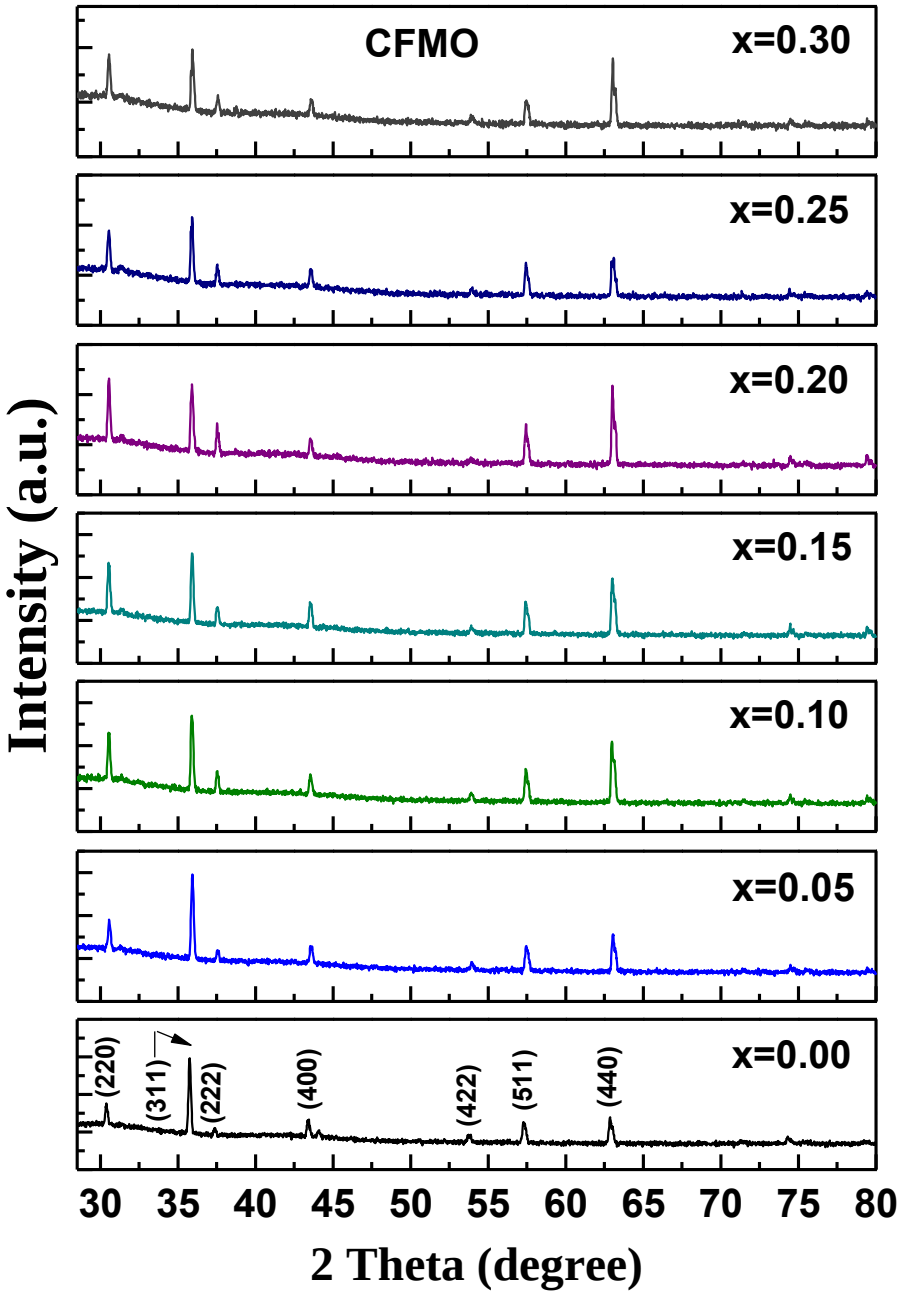
CFMO
x=0.30
x=0.25
x=0.20
x=0.15
x=0.10
x=0.05
x=0.00
(220)
(311)
(222)
(400)
(422)
(511)
(440)
Intensity (a.u.)
30 35 40 45 50 55 60 65 70 75 80
2 Theta (degree)

Figure 2

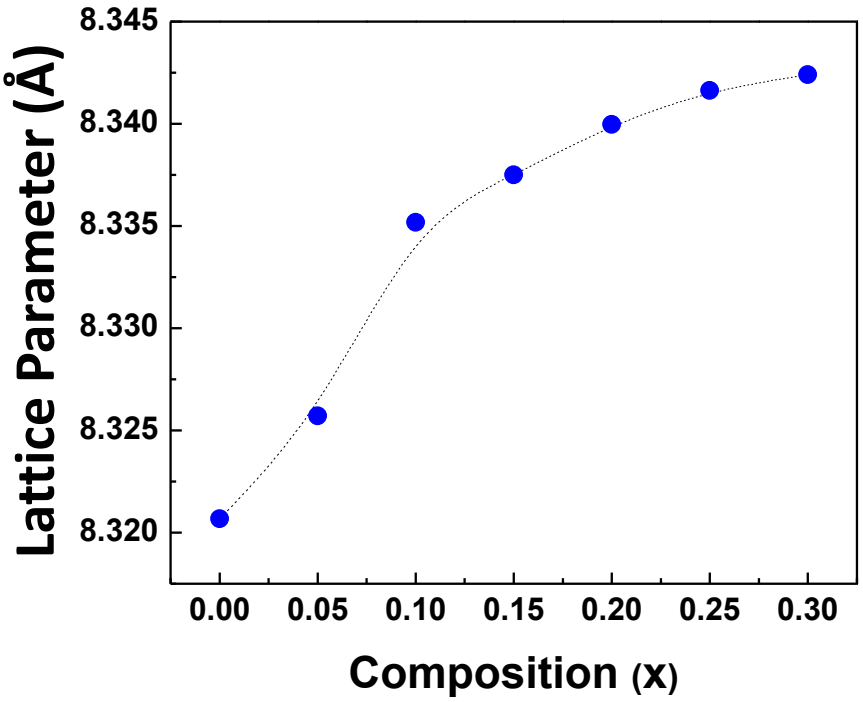
Lattice Parameter (Å)
8.345
8.340
8.335
8.330
8.325
8.320
0.00
0.05
0.10
0.15
0.20
0.25
0.30
Composition (x)

Figure 3 (XPS)

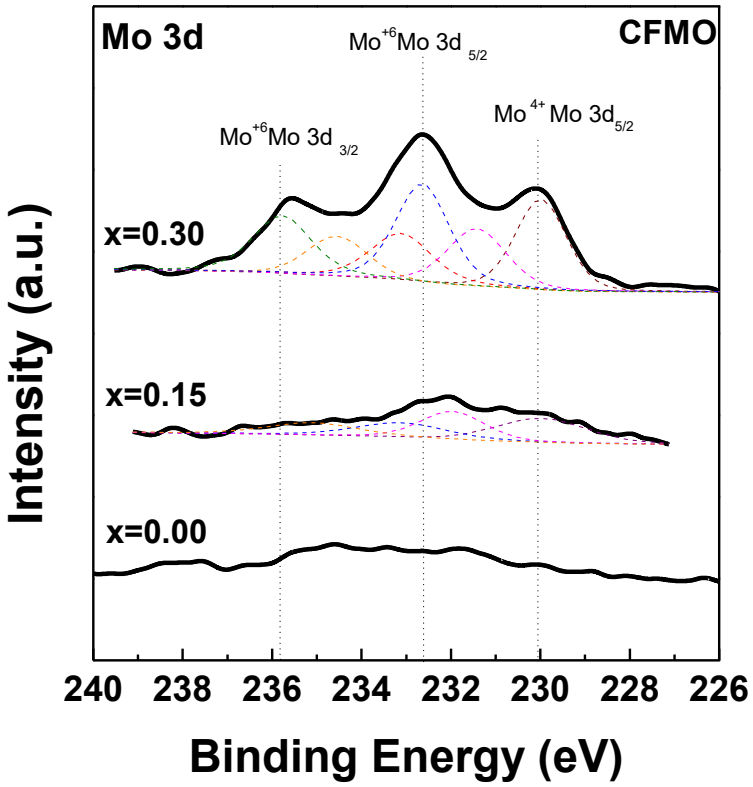
Mo 3d
CFMO
Mo+6Mo 3d 5/2
Mo+6Mo 3d 3/2
Mo 4+ Mo 3d5/2
x=0.30
x=0.15
x=0.00
Intensity (a.u.)
240 238 236 234 232 230 228 226
Binding Energy (eV)

Figure 4

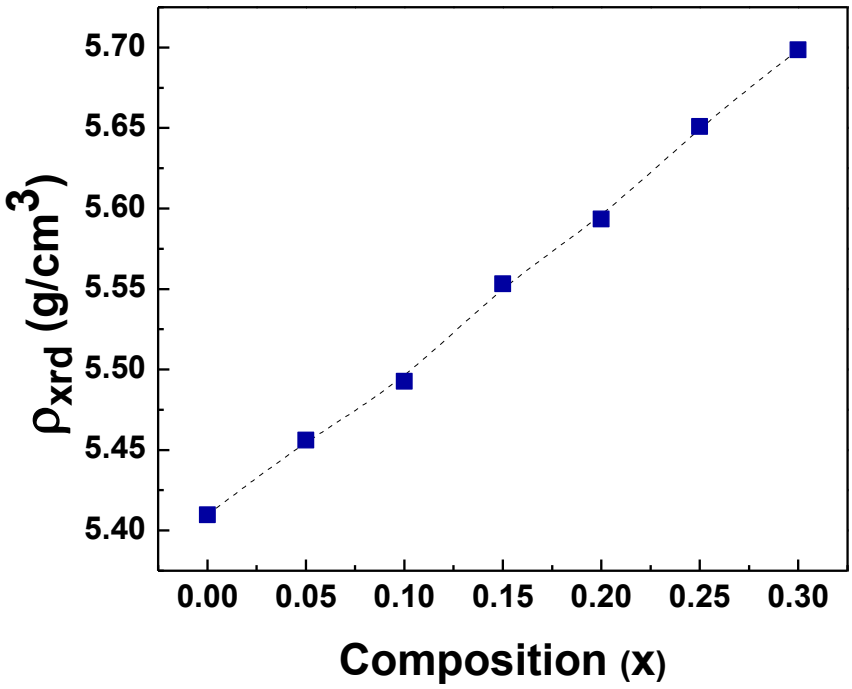
5.70
5.65
5.60
5.55
5.50
5.45
5.40
ρ_{xrd} (g/cm^3)
0.00
0.05
0.10
0.15
0.20
0.25
0.30
Composition (x)

Figure 5

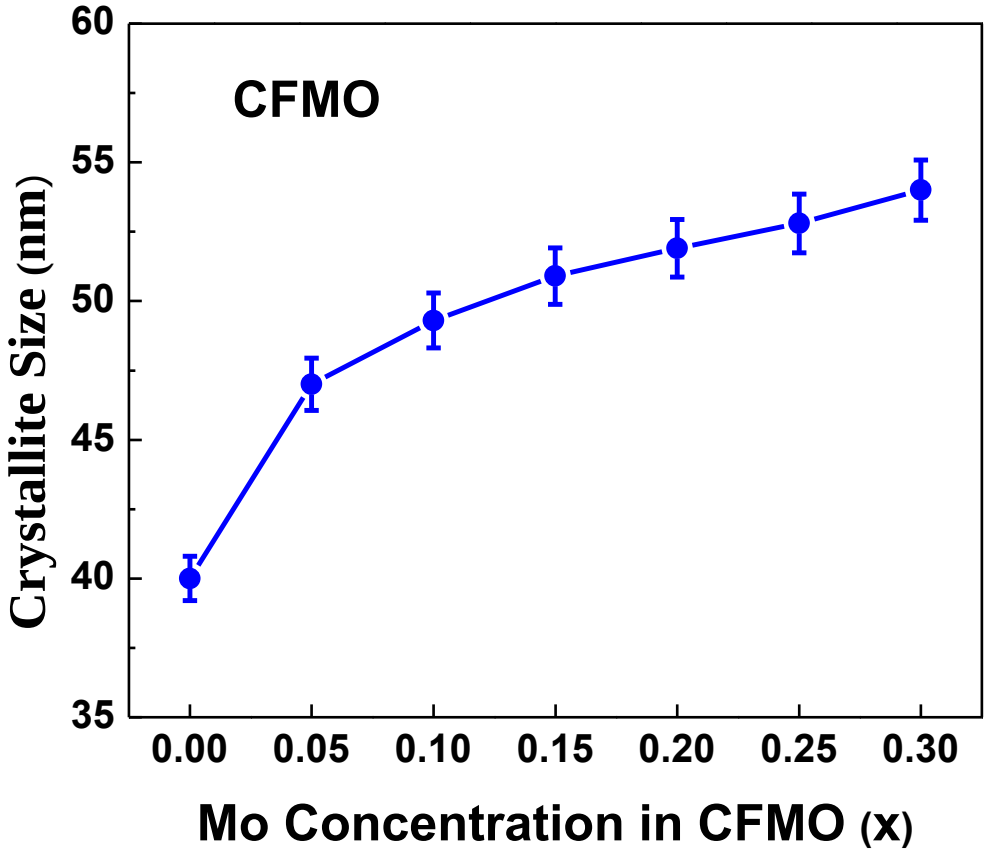
CFMO
Crystallite Size (nm)
60
55
50
45
40
35
0.00
0.05
0.10
0.15
0.20
0.25
0.30
Mo Concentration in CFMO (x)

Figure 6

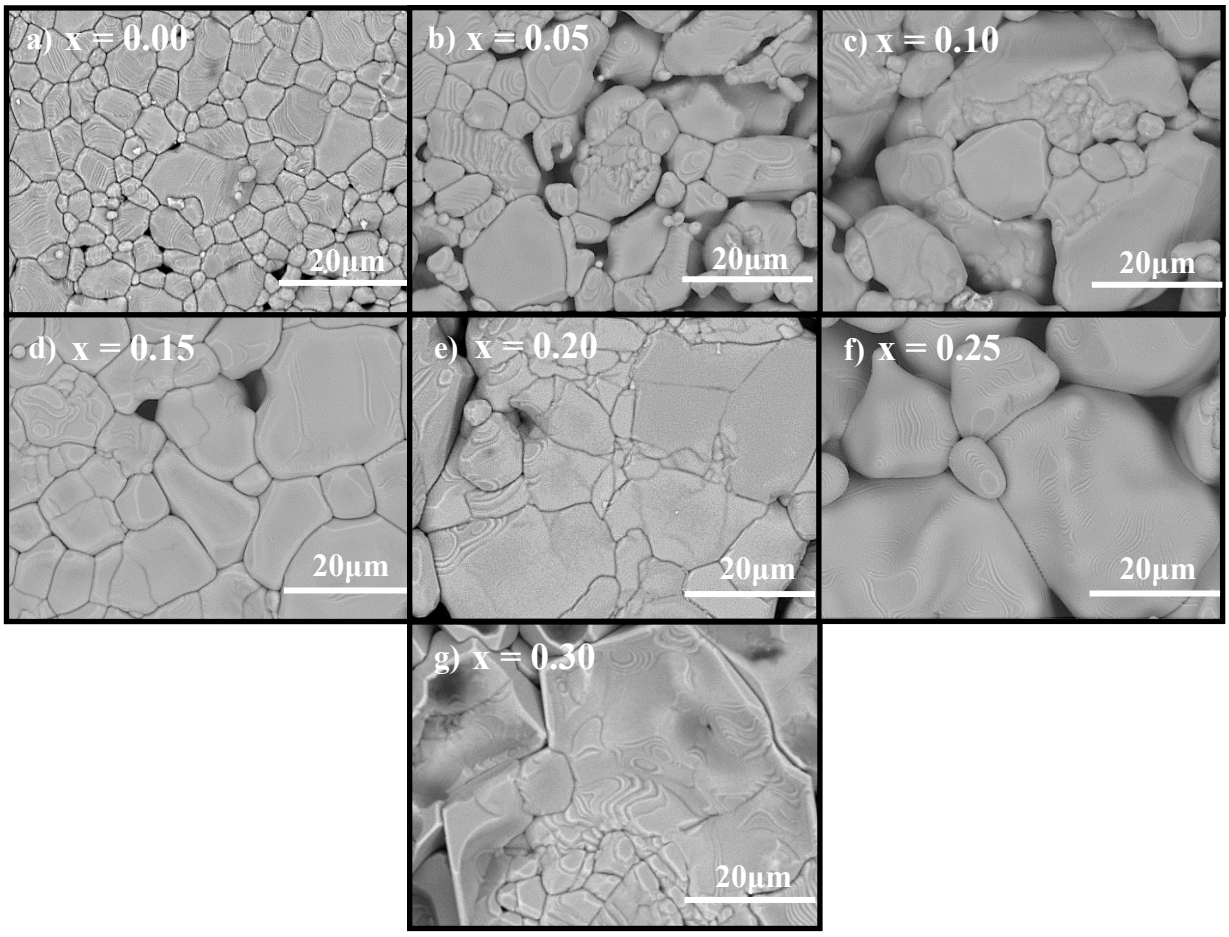
a) x = 0.00
20µm
b) x = 0.05
20µm
c) x = 0.10
20µm
d) x = 0.15
20µm
e) x = 0.20
20µm
f) x = 0.25
20µm
g) x = 0.30
20µm

Figure 7

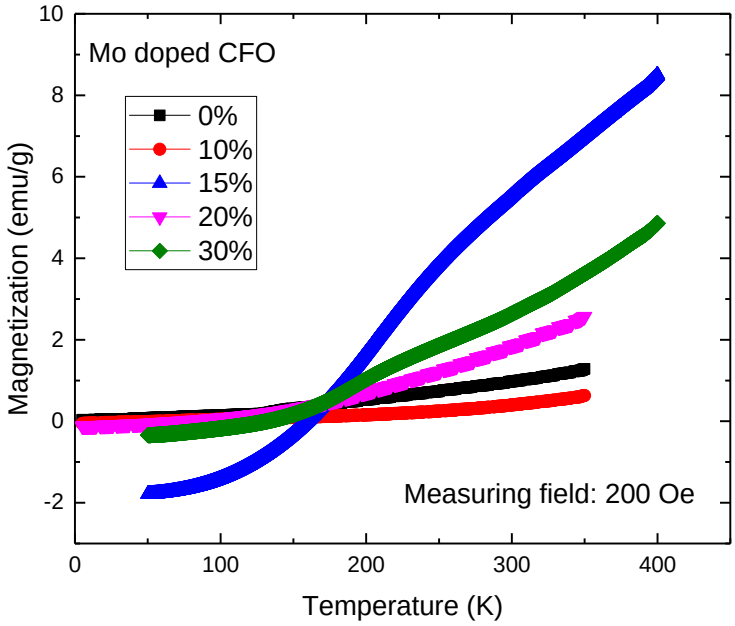
Mo doped CFO
0%
10%
15%
20%
30%
Measuring field: 200 Oe
Magnetization (emu/g)
Temperature (K)
10
8
6
4
2
0
-2
0
100
200
300
400

Figure 8

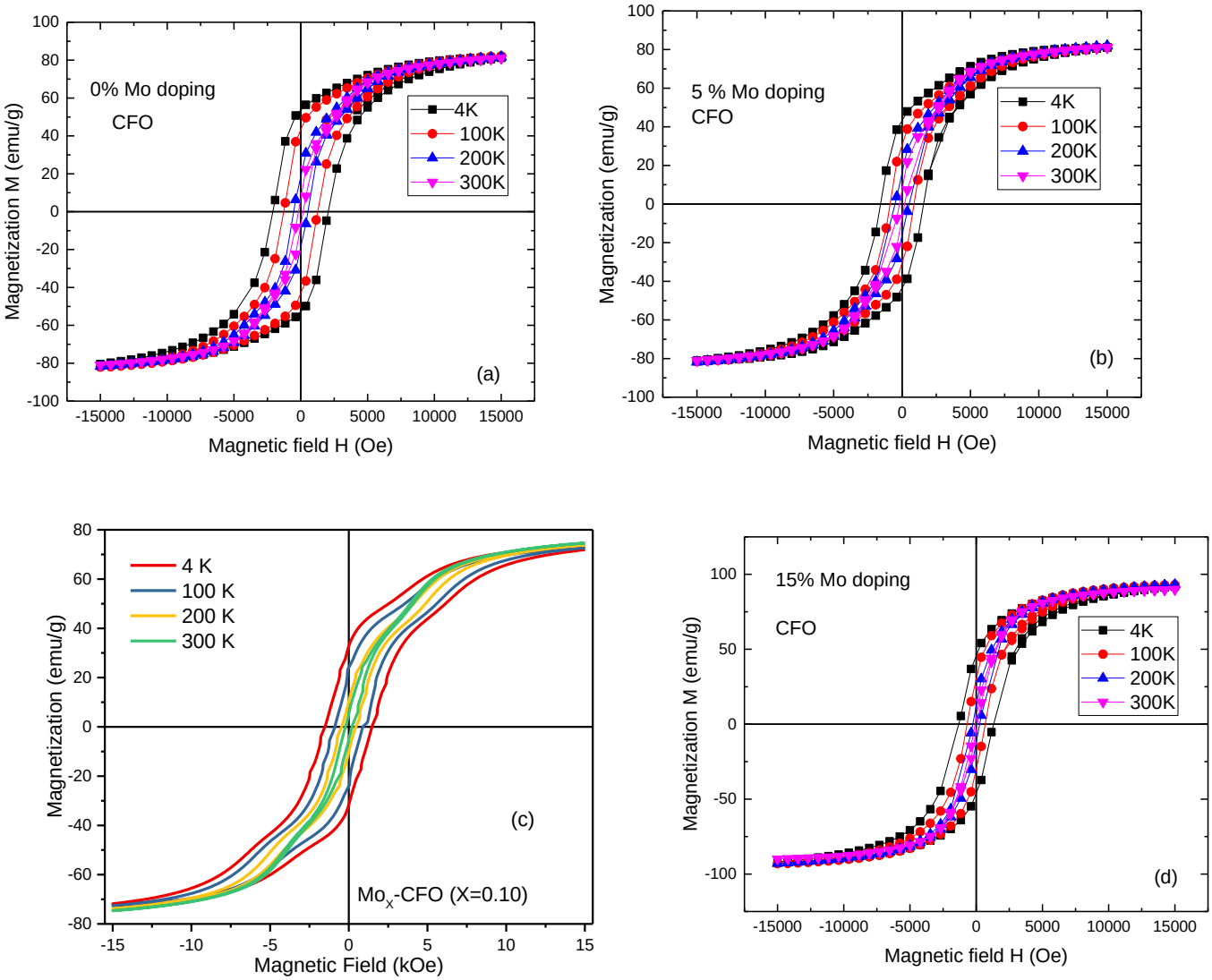
0% Mo doping
CFO
4K
100K
200K
300K
(a)
Magnetization M (emu/g)
Magnetic field H (Oe)
5 % Mo doping
CFO
4K
100K
200K
300K
(b)
Magnetization (emu/g)
Magnetic field H (Oe)
4 K
100 K
200 K
300 K
(c)
Mo$_x$-CFO (X=0.10)
Magnetization (emu/g)
Magnetic Field (kOe)
15% Mo doping
CFO
4K
100K
200K
300K
(d)
Magnetization M (emu/g)
Magnetic field H (Oe)

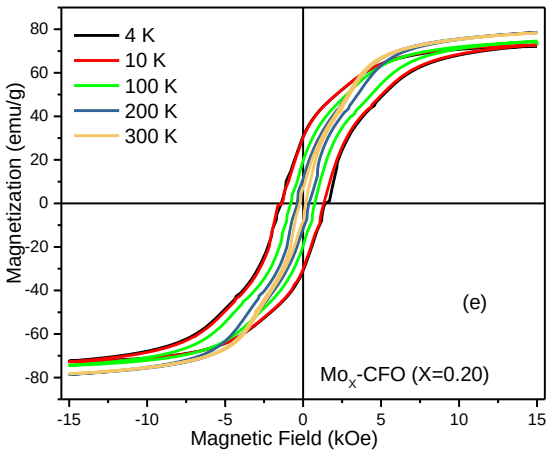
4 K
10 K
100 K
200 K
300 K
Magnetization (emu/g)
Magnetic Field (kOe)
(e)
Mo$_x$-CFO (X=0.20)

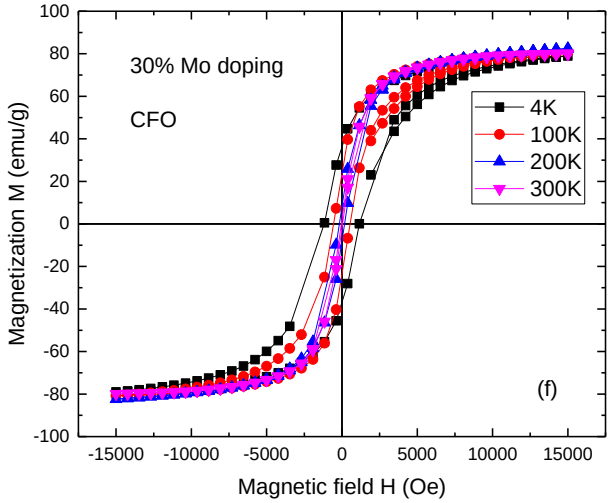
30% Mo doping
CFO
4K
100K
200K
300K
Magnetization M (emu/g)
Magnetic field H (Oe)
(f)

Figure 9

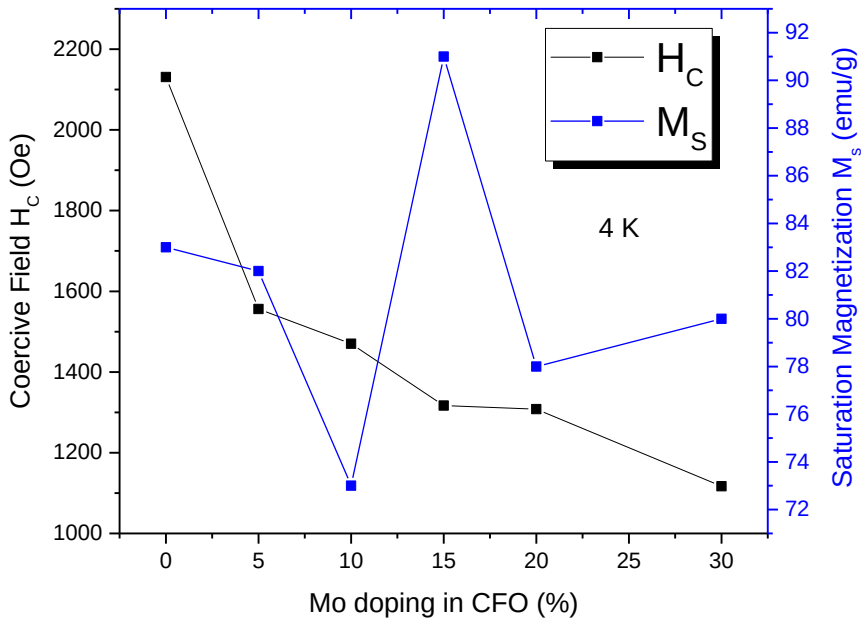
Coercive Field H_C (Oe)
Saturation Magnetization M_s (emu/g)
Mo doping in CFO (%)
H_C
M_S
4 K
2200
2000
1800
1600
1400
1200
1000
92
90
88
86
84
82
80
78
76
74
72
0
5
10
15
20
25
30

Table I

Lattice constant and density of CFMO compounds as function of Mo concentration (*x*).

Mo concentration (*x)* in CFMO	Lattice Constant (Å)	Unit Cell Volume (cm^3/cell)	Effective Density (g/cm^3)
0.00	8.3207	5.7607	5.4097
0.05	8.3257	5.7712	5.4561
0.10	8.3352	5.7909	5.4927
0.15	8.3375	5.7915	5.5532
0.20	8.3399	5.8009	5.5934
0.25	8.3416	5.8045	5.6508
0.30	8.3424	5.8059	5.6985